**Eleventh International Conference on**
**Computational Fluid Dynamics (ICCFD11),**
**Maui, Hawai, USA, July 11-15, 2022**

**ICCFD11-2022-0204**

# Wall-modeled LES of turbulent flow over a two-dimensional Gaussian bump

Prahladh S. Iyer* and Mujeeb R. Malik**
Corresponding author: prahladh.iyer@nianet.org

* National Institute of Aerospace, USA.
** NASA Langley Research Center, USA.

**Abstract:** We perform wall-modeled large eddy simulations (WMLES) of turbulent flow over a nominally two-dimensional Gaussian-shaped bump geometry to assess its performance in the accelerating and separation regions of the flow. The flow conditions are based on high-fidelity numerical simulations of Uzun & Malik (*AIAA Journal 2022*). The oncoming flow Mach number is 0.2, with the bump length-based Reynolds number ($Re_L$) of 2 million. In our previous study, while WMLES with the constant coefficient Vreman subgrid scale model and equilibrium wall model performed satisfactorily at lower $Re_L = 1$ million, it failed to predict flow separation at the higher $Re$, contrary to the experimental observations. We investigate the sensitivity of WMLES to different subgrid scale models, wall models, and grid resolution and topology on flow separation by comparing with available data.

*Keywords:* Computational Fluid Dynamics (CFD), Turbulence, Flow Separation, Large Eddy Simulation (LES).

## 1 Introduction

Wall-modeled large eddy simulation (WMLES) methods are becoming increasingly popular for high Reynolds number turbulent flow configurations with separation, due to their potential to be more accurate compared to Reynolds-averaged Navier-Stokes simulations (RANS), which are the current industry standard. While the RANS technique models all of the turbulence scales, the WMLES technique resolves a significant portion of the energy-carrying eddies away from the wall. Thus, grid refinement in WMLES is likely to lead to more accurate predictions, while the modeling error, which dominates in RANS, is independent of the grid resolution. Nevertheless, the current framework and models used in WMLES are far from perfect; further understanding and improvements are necessary to enable their use for complex industrial applications.

The wall-modeled LES approach, in which the near-wall region is modeled with RANS, while the majority of the length scales away from the wall are resolved using LES, is a reasonable compromise between accuracy and computational cost. Wall-modeled LES can further be classified into (i) stress-based WMLES, and (ii) hybrid RANS/LES methods such as Improved Delayed Detached Eddy Simulation (IDDES). In the stress-based WMLES approach, the computational grid is coarse in the wall-normal and wall-parallel directions, thus requiring the regular no-slip boundary condition to be supplemented by wall shear stress and heat flux/ temperature boundary conditions. See Cabot & Moin [1], Piomelli & Balaras [2], Larsson et al. [3] and Bose & Park [4] for overviews of stress-based WMLES. In IDDES, the grid is very fine in the wall-normal direction but coarse in the wall-parallel direction thus requiring the LES eddy viscosity to be replaced by a RANS eddy viscosity where the majority of the turbulence is modeled. See Spalart [5], Deck [6], Spalart et al. [7] and Shur et al. [8] for an overview of the DES-based approach. In this study, we focus on the stress-based WMLES approach, which is implied when we refer to WMLES in the rest of the paper.

The experimental configuration of the Gaussian bump was proposed by experts at Boeing [9] in order to provide validation data for smooth-body flow separation. Some preliminary experiments were performed by Williams et al. [10] for this configuration at Reynolds numbers ($Re_L$) between 1.3 and 3.4 million based on the length of the bump ($L$). More detailed experiments are being conducted at the University of Notre Dame [11]. Uzun & Malik [12] have performed Direct Numerical Simulation (DNS) for the nominally two-dimensional spanwise-periodic configuration at $Re_L = 2$ million with a detailed analysis of the flow physics in the favorable and adverse pressure gradient regions of the flow. DNS have also been performed by multiple groups at a lower $Re_L = 1$ million [13, 14, 15], where the boundary layer undergoes partial relaminarization in the favorable pressure gradient region of the bump. Balin et al. [14] performed IDDES-based WMLES for this configuration at $Re_L = 1$ million with valuable insights into the flow. Their results indicate that WMLES performance deteriorates as one moves from the favorable to adverse pressure gradient regions of the flow, with larger errors in the separated region of the flow. The stress-based WMLES framework used in the present study has shown promising results in our previous studies such as flow over a wall-mounted hump [16], transonic flow past an axisymmetric bump [17], and supersonic flow past a compression ramp [18]. We have previously performed WMLES of the spanwise periodic and full three-dimensional configurations at $Re_L = 1$ and 3.6 million [19] using an unstructured finite-volume solver and the equilibrium wall model. Comparisons with DNS data at $Re_L = 1$ million showed good agreement overall, with a reduced tendency to separate. Note that relaminarization was not captured in WMLES. At the higher $Re_L = 3.6$ million, both the spanwise periodic and three-dimensional results were qualitatively similar and did not predict any flow separation, in contrast to the experimental observations of Williams et al. [10]. More recently, Whitmore et al. [20] and Agrawal et al. [21] report the effects of different wall models and subgrid models, respectively, for the $Re_L = 2$ million configuration. By comparing to high-fidelity numerical data from Uzun & Malik [12], we perform detailed sensitivity studies with WMLES at $Re_L = 2$ million in the present study to understand the errors and suggest possible improvements.

The paper is organized as follows. The details of the flow solver and wall model are briefly discussed in Section 2. The flow configuration, grid, and simulation details are discussed in Section 3. WMLES results are discussed in Section 4, and the results are summarized in Section 5.

# 2 Numerical Details

The *CharLES* solver[*] is used in the simulations. The compressible solver discretizes the Navier-Stokes equations on unstructured grids using a cell-centered finite-volume methodology. The baseline solver is second-order accurate in space for unstructured grids with an explicit third-order Runge-Kutta time advancement scheme. Two versions of the solver are used; one with hexahedral-dominant extruded grids [22, 23] , and another with polyhedral Voronoi grids [24, 25]. While both versions have low numerical dissipation, the spatial discretization is not identical. The constant coefficient Vreman model [26] or the dynamic Smagorinsky model [27, 28] are used to model the subgrid scale contributions, and the equilibrium wall model [29] is used to prescribe the wall shear-stress in most of the results presented.

# 3 Problem Description

The experimental configuration described in Slotnick [9] consists of a symmetric Gaussian-shaped bump in the center of the wind tunnel ($z = 0$) with a length and width $L$, that extends to the sides of the tunnel ($z/L = \pm 0.5$). It is attached to a flat plate section both upstream and downstream of the bump ($|x/L| > 0.5$), and tapered along the spanwise direction ($z$) to minimize side-wall interference effects. In this study, we focus on the spanwise periodic configuration, which is based on the shape of the bump in the symmetry plane ($z = 0$), and described by the following equation:

$$y(x, z) = \frac{h_0}{2} e^{-\left(\frac{x}{x_0}\right)^2} \tag{1}$$

Here, $x$ and $y$ are the streamwise and wall-normal directions of the oncoming boundary layer. The constants $x_0 = 0.195L$ and $h_0 = 0.085L$ are used. The bump shape is invariant with the spanwise direction ($z$).

---

[*] Cascade Technologies, Webpage: `http://www.cascadetechnologies.com` [Last accessed: June 15, 2022]

The freestream Mach number is 0.2, and the freestream Reynolds number based on the bump length ($L$) is 2 million, consistent with the DNS of Uzun & Malik [12]. The boundary-layer thickness of the oncoming turbulent boundary layer ($\delta_{in}$) is $\approx 0.0085L$ at $x/L = -0.65$ for $Re_L = 2$ million, which is used as a reference to construct the WMLES grid. Note that the boundary-layer thickness varies considerably over the bump, with a value of 0.018 at $x/L = -0.2$ and $\approx 0.05$ at $x/L = 0.2$ [12]. Two types of grids are used in this study. The first grid is extruded along the span with constant spanwise spacing, and is composed of primarily hexahedral elements. A snapshot of the grid is shown in Figure 1. This grid corresponds to the medium resolution grid used in Iyer & Malik [19], and contains about 16 million cells for a span of $0.04L$. Within the boundary-layer region, the grid is mostly isotropic with a spacing of $\Delta = 0.0005L$. The first wall-normal spacing is half the value ($0.00025L$), with the second off-wall grid point used as the exchange location at which data are input to the wall model. The grid spacing of $0.0005L$ corresponds to $\approx 17-18$ points per boundary layer thickness at $x/L = -0.65$, and a viscous wall spacing of $\approx 40$ at $x/L = -0.5$, and $\approx 68$ at $x/L = 0$ computed using the skin friction data from the DNS of Uzun & Malik [12]. The second grid contains isotropic polyhedral Voronoi elements, and was generated using the *Stitch* utility in *CharLES*[†]. This grid contains isotropic elements with spacings varying between $0.00027L$ at the wall to $0.0043L$ in the farfield. This grid has a wall-parallel spacing of $0.00027L$ in the near-wall region that is finer than the hexahedral-dominant grid by approximately a factor of two. This grid is similar in design to the grid used by Whitmore et al. [20], and contains about 25 million cells for a span of $0.04L$. The first grid point is used as the exchange location for results using this grid. Note that these grids are over two orders of magnitude coarser than the DNS grid used by Uzun & Malik [12] that contains about 10.2 billion points for a span of $0.08L$.

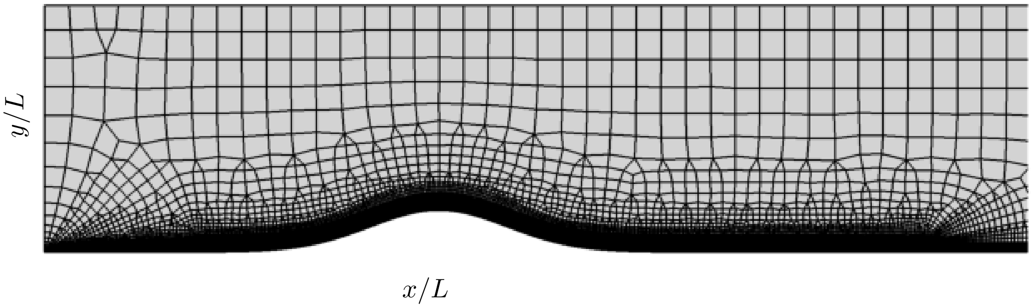

Figure 1: A snapshot of the unstructured grid used in WMLES is shown at $z = 0$.

The reference DNS of Uzun & Malik [12] placed the top boundary at $y/L = 1$ and imposed freestream conditions. Our WMLES results obtained using the hexahedral-dominant grid had the top boundary located at $y/L = 0.5$ with freestream conditions, and were run with a span of $0.04L$ (half the span of DNS), but the differences in the tendency to separate appears to be small for both factors as discussed in Section 4.2. The inflow was placed at $x/L = -0.67$, and synthetic turbulence was prescribed based on time-averaged flow from Reynolds-averaged Navier-Stokes (RANS) results using the Spalart-Allmaras (SA) model for the hexahedral-dominant grid, and from the reference DNS for the polyhedral Voronoi grid. The differences between using a RANS and DNS are small as quantified in Iyer & Malik [19] for $Re_L = 3.6$ million. An absorbing sponge boundary condition [30] is used at the outflow for $x/L > 1$, with the freestream value specified for the pressure. The equilibrium wall model boundary condition is imposed at the wall, with periodic boundary conditions along the span. All the simulations were run between 5 and 10 $L/u_\infty$, and the statistics were collected for about 5 and 10 $L/u_\infty$.

---

[†] Cascade Technologies, Webpage: `http://www.cascadetechnologies.com` [Last accessed: June 15, 2022]

# 4 Results

## 4.1 Unstructured 16 Million Grid

We report WMLES results using the 16 million hexahedral-dominant grid discussing the effect of subgrid scale (SGS) model coefficient for the static Vreman model, the use of a nonlinear SGS model, and finally the nonequilibrium wall model by detailed comparisons with the reference DNS data. Note that the top boundary was placed at $y/L = 0.5$ in WMLES with a span of $0.04L$, compared to $y/L = 1$ and a span of $0.08L$ in DNS. Thus, an exact quantitative match is not expected, although these effects are small as discussed in Section 4.2. The equilibrium wall model is used for the results discussing the effect of the SGS model. The aim of the sensitivity studies in this Section is to evaluate whether improved predictions can be observed on a given medium resolution grid, rather than improve predictions by grid refinement.

### 4.1.1 Effect of Vreman Subgrid Scale Model Coefficient

The constant coefficient Vreman SGS model with $c = 0.07$ [26] has been used in a number of previous studies with reasonable success, especially in the wall-resolved LES regime. For WMLES, where the grid resolutions are typically much coarser (at least by a factor of 2-4 in each direction depending on the $Re$), the model performance needs to be assessed more carefully, especially in challenging flow regimes such as smooth-body separation. We vary $c$ between 0 (no SGS model) and 0.07 for this configuration, and compare the results with the dynamic Smagorinsky model (DSM) in Figure 2. The results indicate a monotonic trend with respect to separation, with the smaller values of $c$ yielding more separation for this grid and flow conditions, and the standard value yielding no flow separation. The DSM model results are close to the standard Vreman coefficient value of 0.07. The optimal value is likely a function of the grid resolution, and flow conditions such as Reynolds number. An instantaneous snapshot of the horizontal velocity contour is shown for $c = 0.07$ and 0.025 in Figure 3. A large separation bubble is observed for the lower $c$ value, while very mild separation is observed for the standard value. Note that no separation is observed for the standard coefficient model in the time-averaged flowfield.

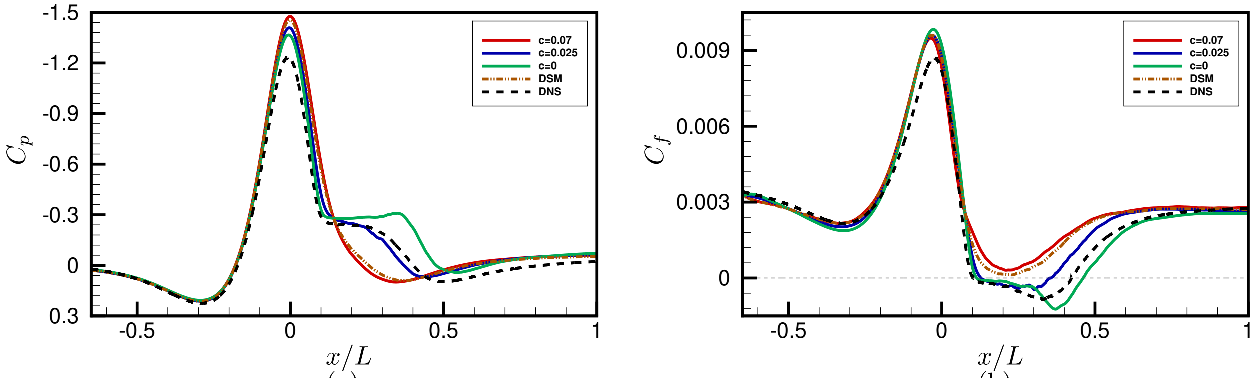

(a) (b)

Figure 2: The variation of wall pressure (a) and skin friction (b) is compared to DNS for different Vreman SGS model coefficients and the DSM model.

Figure 4 depicts the variation of time-averaged velocity and the total turbulent shear-stress (resolved + modeled) profiles with the vertical distance from the wall ($y-$direction) at three stations corresponding to $x/L$ =-0.4, -0.2, 0 and 0.2. Note that the flow separates at $x/L \approx 0.1$ in the DNS. Also, WMLES data for $y/L < 0.0005$ (below the exchange location) are not expected to be accurate due to the lack of grid resolution in that region based on the reasoning of Kawai & Larsson [29]. The velocity profiles are similar for the different coefficient values at the first two stations, while the total turbulent shear-stress profiles show some differences. At $x/L = -0.4$ where the flow is attached and the pressure gradient is small, $c = 0.07$ and the DSM model results agree best with DNS. A similar qualitative trend is observed at $x/L = -0.2$. However, as we reach the apex of the bump ($x/L = 0$), the trend changes with $c = 0.025$ being closest to

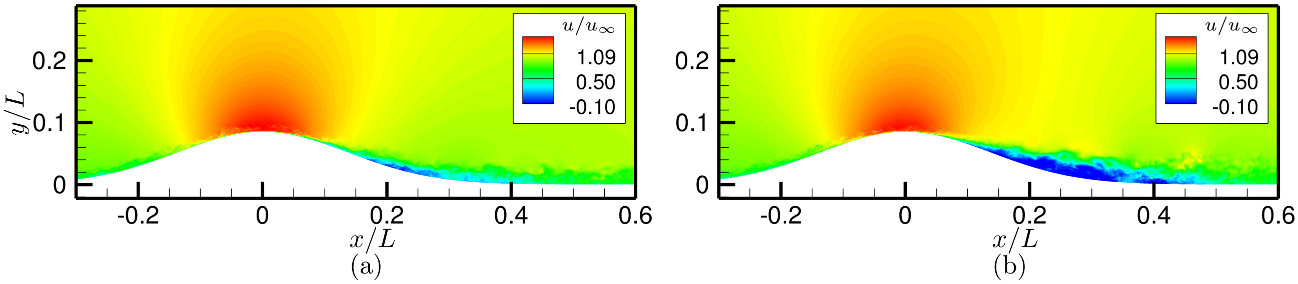

Figure 3: WMLES results showing instantaneous horizontal velocity contour with the Vreman SGS model coefficient of (a) 0.07 and (b) 0.025.

DNS beyond $y/L = 0.0005$. However, the velocity profile of $c = 0$ is closest to DNS at $x/L = 0$. Note that the wall pressure and skin-friction variation were closest to DNS for $c = 0.025$ in Figure 2, indicating a strong correlation between the separation length and the turbulent profiles upstream of separation. At $x/L = 0.2$, which lies inside the separation bubble in the DNS, $c = 0$ is closest to DNS. Further grid sensitivity is likely required to extract clear trends, although it is clear that on this grid, the subgrid model coefficient has a significant effect on predicting flow separation.

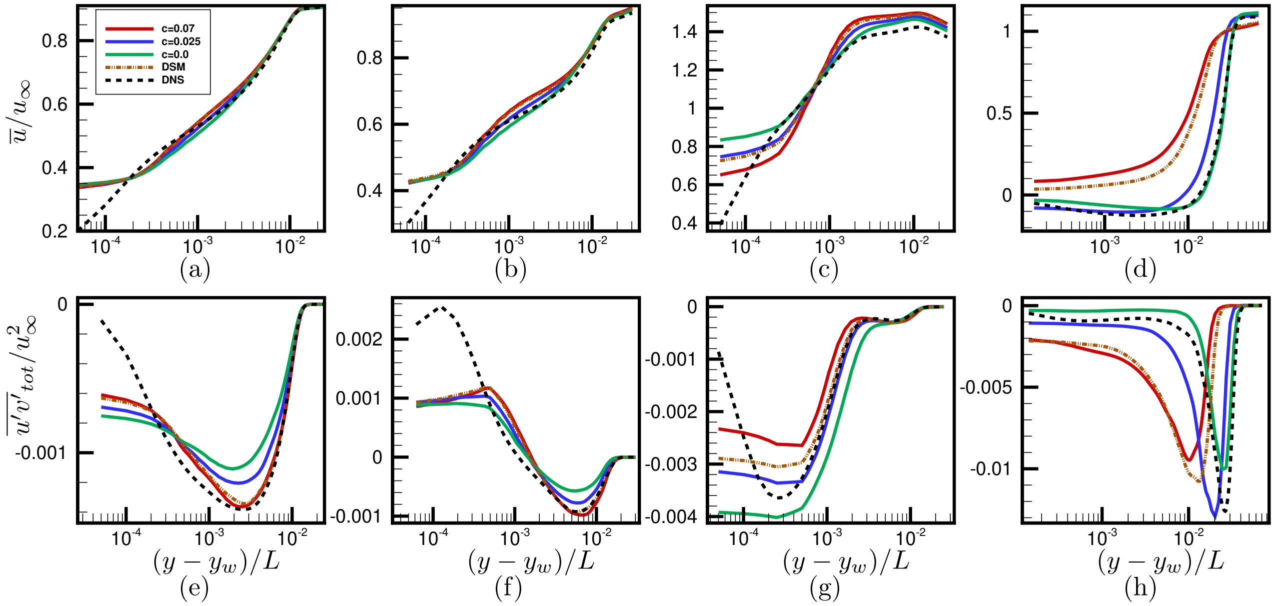

Figure 4: The variation of time-averaged horizontal velocity ($\overline{u}$, Figures a-d), and total turbulent shear stress ($\overline{u'v'}$, Figures e-h) at constant horizontal stations are shown for the different Vreman SGS model coefficients and the DSM model at $x/L$ =-0.4 (a,e), -0.2 (b,f), 0 (c,g) and 0.2 (d,h).

### 4.1.2 Effect of Nonlinear Subgrid Scale Model

The Vreman and DSM models used in the previous section use an isotropic eddy viscosity, and assume that the modeled SGS stresses are aligned with the strain-rate tensor. This assumption does not hold in general for complex flows, especially for coarse grid resolutions used in WMLES. We assess the performance of a nonlinear SGS model, which could potentially capture anisotropy in the modeled SGS stresses. We use the Explicit Algebraic Subgrid Stress Model (EASSM) of Marstorp [31], which depends on the SGS kinetic energy, and a nonlinear combination of the strain and rotation rate tensors. The SGS kinetic energy is computed dynamically using the Yoshizawa model [32] and Germano identity [27], while the other constants in the model are dependent on flow quantities such as the filtered strain or rotation rate tensor. Rasam et al. [33, 34] obtained improved results with the EASSM model for wall-resolved LES of separated flow on coarser grids compared to the DSM model. Figure 5 depicts the variation of wall pressure and skin-friction for the EASSM model and the Vreman SGS model (with $c = 0.07$), and we observe that the EASSM model predicts flow separation and agrees well with DNS in contrast to the Vreman model.

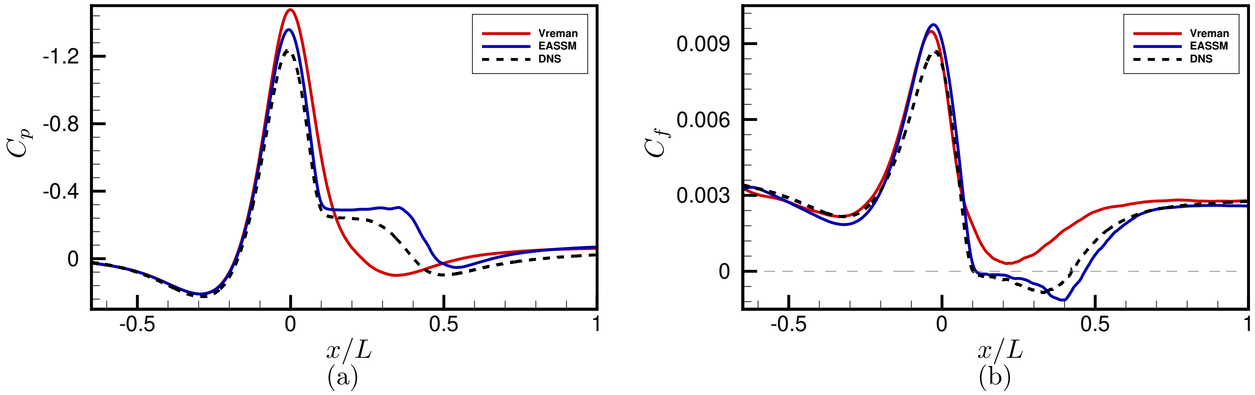

Figure 5: The variation of (a) wall pressure and (b) skin friction is compared to DNS for the standard Vreman and EASSM SGS models.

Figure 6 depicts the variation of time-averaged velocity and resolved turbulent stresses at $x/L = -0.4$ and 0. The differences in velocity are small between the two models at $x/L = -0.4$ as observed in Figure 4, while the resolved stresses show some differences. Interestingly, the Vreman model agrees better with DNS in terms of stresses, which could be due to the improved $C_f$ prediction observed at this location compared to the EASSM model. Also, the magnitude of $\overline{u'u'}$ and $\overline{u'v'}$, which scales with the local skin-friction coefficient, is better predicted by the Vreman model. At $x/L = 0$, the EASSM model is closer to DNS for both velocity and the turbulent stresses, which correlates with the separation prediction further downstream. While preliminary results are encouraging, further evaluation on finer grids and different $Re$ is necessary for the nonlinear EASSM model.

### 4.1.3 Effect of Nonequilibrium Wall Model

Thus far, all the results used the equilibrium wall model that neglects nonequilibrium effects such as strong favorable and adverse pressure gradients, which are present in this flow. We compare the results using the nonequilibrium wall model of Park & Moin [35]. The DSM model is used for both the wall models. Figure 7 shows the variation of wall pressure and skin-friction using the two wall models, and while the nonequilibrium wall model is marginally better, it does not predict a significant amount of separation as observed in the DNS similar to what was observed by changing the SGS model coefficient or by the use of a nonlinear SGS model. These results suggest that varying model parameters away from the wall (such as SGS model) has a greater influence on the separation characteristics for this flow configuration.

## 4.2 Results: Polyhedral Voronoi Grid

WMLES results using the polyhedral Voronoi grid containing 25 million cells for a span of $0.04L$ showing the effect of grid resolution, spanwise domain width, top boundary location and turning off the wall model are discussed. The time-averaged velocity and turbulent stresses from DNS are used to generate synthetic turbulence at the inflow ($x/L = -0.67$). The equilibrium wall model and DSM SGS model was used for all the results presented in this section.

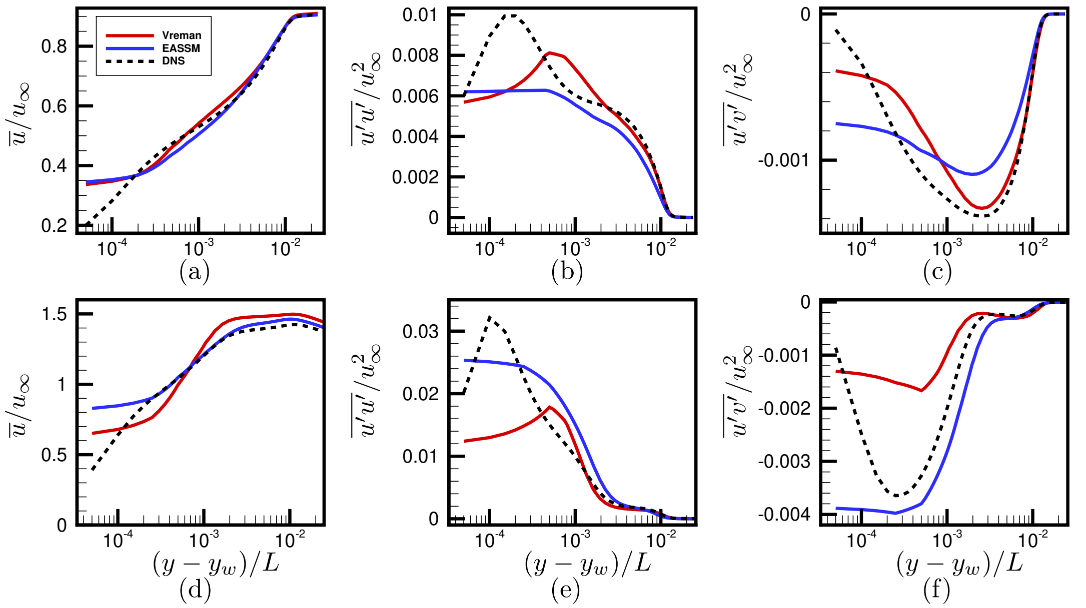

Figure 6: The variation of time-averaged horizontal velocity ($\overline{u}$, Figures a,d), and resolved turbulent stresses ($\overline{u'u'}$, Figures b,e and $\overline{u'v'}$, Figures c,f) at constant horizontal stations are shown for the standard Vreman and EASSM SGS models at $x/L$ = -0.4 (a-c) and 0 (d-f).

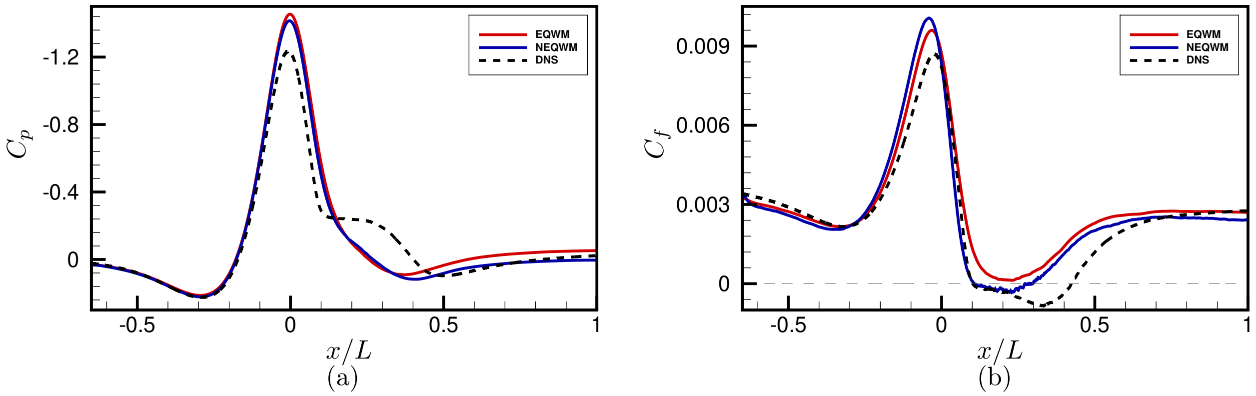

Figure 7: The variation of wall pressure (a) and skin friction (b) is compared to DNS for the equilibrium and nonequilibrium wall models using the DSM SGS model.

### 4.2.1 Effect of Grid Resolution

To study the effect of grid resolution in the near-wall region, we coarsen the region by a factor of 2 until $0.004L$ away from the wall to make the minimum grid spacing equal to $0.00054L$ (comparable to the wall-parallel spacing of the 16 million hexahedral-dominant grid used in Section 4.1), which extends to a distance of $0.012L$ away from the wall. This coarser grid contains 9 million cells for a span of $0.04L$ compared to 25 million cells for the baseline grid, and differs only in the region within $0.004L$ of the wall. Figure 8 shows the variation of wall pressure and skin-friction comparing the coarse and fine WMLES grid results with DNS. The results indicate the grid resolution in the thin region close to the wall has a significant impact on the separation characteristics, with the finer grid showing excellent agreement with DNS, and the coarser grid showing no separation similar to the 16 million unstructured hexahedral-dominant results. Uzun & Malik [12] suggest that resolving the thin internal layer may be critical to capturing flow separation, and the qualitative trend observed here appears to be consistent with their reasoning, although further analysis is required regarding how well the internal layer is captured on this 25 million grid.

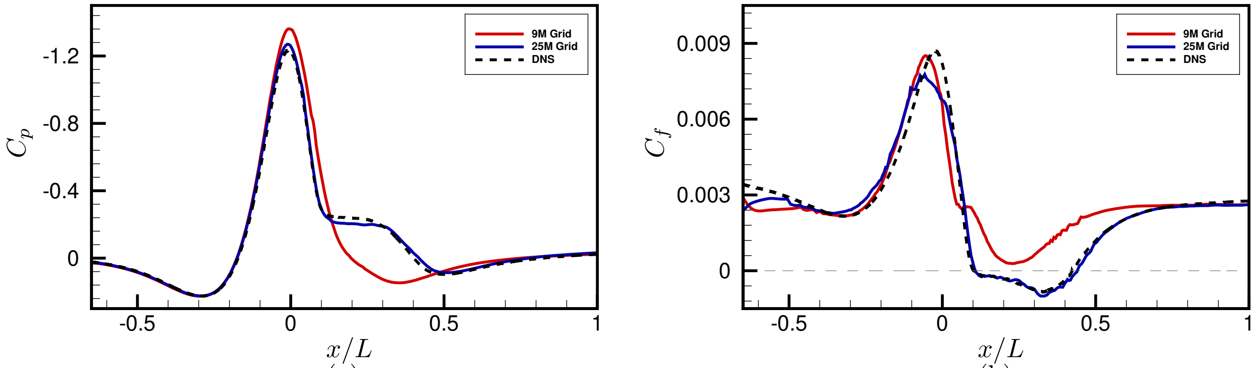

(a) (b)

Figure 8: The variation of (a) wall pressure and (b) skin friction is compared to DNS for the 9 and 25 million polyhedral grids.

### 4.2.2 Effect of Spanwise Domain Width

We report the effect of spanwise domain size by comparing the results with $0.04L$ and $0.08L$ width, with the grid containing 25 and 50 million cells, respectively. Note that the DNS had a spanwise width of $0.08L$. The variation of wall pressure and skin-friction is shown in Figure 9, and indicate that the spanwise domain size has a nonnegligible effect on the separation size. The wider span predicts a slightly smaller separation bubble, which is qualitatively consistent with the observations by Shur et al. [15] for the $Re_L = 1$ million case. While one might expect the wider span result to match better with DNS due to the consistent spanwise extent, the narrow span result agrees better, which could be fortuitous and due to cancellation of other WMLES errors.

The time-averaged velocity and resolved turbulent stresses are compared in Figure 10 at $x/L$ =-0.4, -0.2, 0 and 0.2. The effect of span appears to be small until $x/L = 0$, with minor differences in stresses in the near-wall region. Larger differences are observed inside the separation bubble at $x/L = 0.2$, with respect to the location of the separated shear layer corresponding to the region around the maximum stresses and the magnitude of the stresses. The results indicate that spanwise confinement reduces the unsteadiness of the separated shear layer. Some small differences in the turbulent stress profiles (and lack of smoothness) could be attributed to the smaller averaging time used for the narrow span result. Note that the profiles are only time-averaged and not spanwise-averaged here. The results at $x/L = 0.2$ indicate that further grid refinement in this region may be necessary to improve predictions as the separated shear-layer away from the wall, with lesser wall model influence compared to attached regions, would likely have a dominant influence.

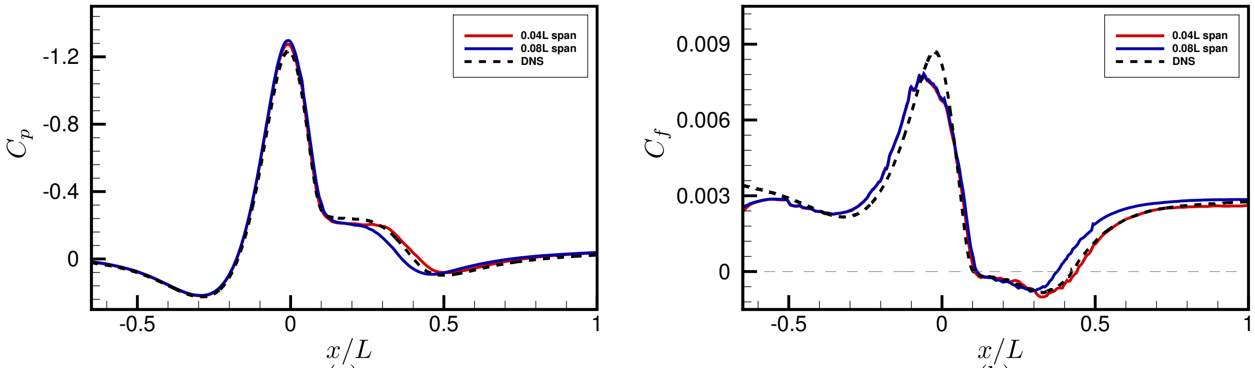

(a) (b)

Figure 9: The variation of (a) wall pressure and (b) skin friction is compared to DNS for polyhedral grid for a span of $0.04L$ and $0.08L$.

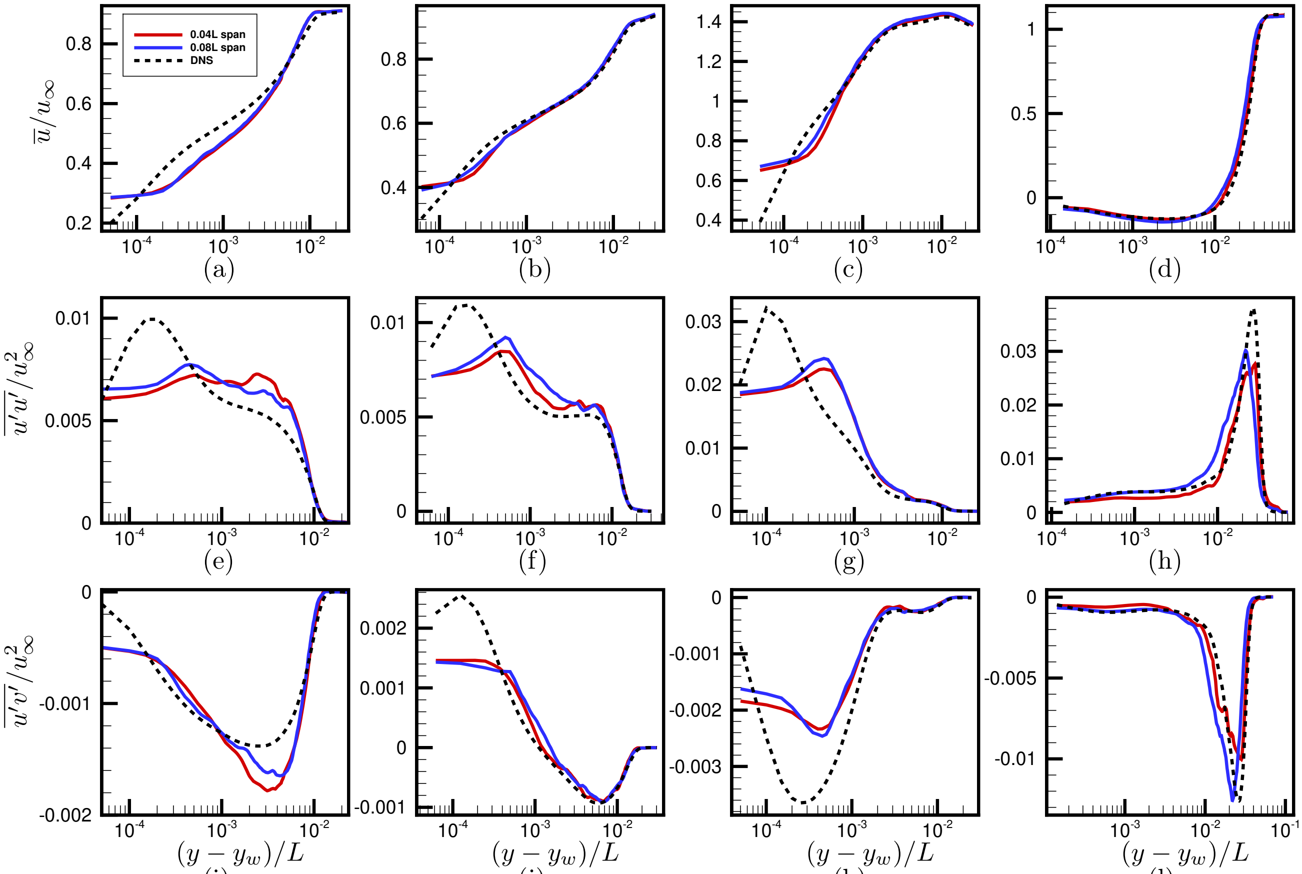

(a) (b) (c) (d)

(e) (f) (g) (h)

(i) (j) (k) (l)

Figure 10: The variation of time-averaged horizontal velocity ($\overline{u}$, Figures a-d), and resolved turbulent stresses ($\overline{u'u'}$, Figures e-h and $\overline{u'v'}$, Figures i-l) at constant horizontal stations are shown for a span of $0.04L$ and $0.08L$, at $x/L$ = -0.4 (a,e,i), -0.2 (b,f,j), 0 (c,g,k) and 0.2 (d,h,l).

#### 4.2.3 Effect of Top Boundary Location

The effect of the top boundary location imposed with freestream conditions for the 0.08L span, 50M grid is assessed. Figure 11 depicts the variation of wall pressure and skin friction for the top boundary located at 0.5L and 1L. Due to larger confinement at $x/L = 0$ for the 0.5L case, the inviscid flow moves faster and produces a lower pressure here. This is seen in the wall pressure variation with the 1L top wall WMLES result agreeing better with DNS. The effect on skin friction is minimal until close to $x/L \approx -0.1$, beyond which there exists a moderate effect due to the pressure being affected by the top boundary location. Top boundary confinement appears to slightly reduce the size of the separation bubble.

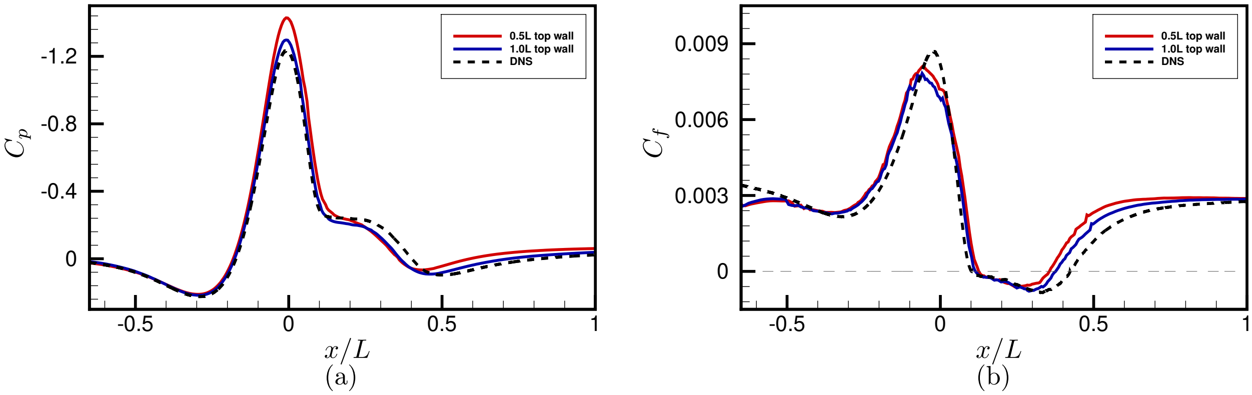

(a)
(b)

Figure 11: The variation of (a) wall pressure and (b) skin friction is compared to DNS for polyhedral grid for the top boundary located at $0.5L$ and $1L$.

#### 4.2.4 Effect of Turning Off the Wall-Model

Lastly, we report the effect of turning off the wall model on the 25M grid and 0.04L span to see if any flow separation is predicted on this grid and setup. Figure 12 depicts the influence of turning off the wall model on the wall pressure and skin friction. All parameters except the boundary condition at the wall are kept identical between the two results shown in the figure, with the equilibrium wall model used in one case, and the no-slip model used in the other. Note that no wall-normal grid refinement was performed for the no-slip result although the first grid point lies beyond the viscous sublayer. The deterioration of wall pressure and skin friction is small until $x/L \approx -0.1$; however, the differences are large beyond this region, with the no wall model result not predicting any flow separation. Thus, the influence of the wall model on this grid significantly contributes to predicting separation.

## 5 Summary

Wall-modeled LES was performed for the spanwise periodic configuration at $Re_L = 2$ million to assess its ability to predict separation with modest grid requirements. The sensitivity of WMLES predictions to different subgrid models (Vreman model with different coefficients, Dynamic Smagorinsky model), wall models (equilibrium and nonequilibrium) and grid resolutions and topology (hexhedral-dominant, polyhedral) were assessed based on detailed comparisons to the high-resolution reference DNS data of Uzun & Malik [12]. Encouraging results were observed by reducing the subgrid model coefficient for the Vreman model, and improved predictions were observed with the nonlinear Explicit Algebraic Subgrid Scale Model (EASSM) of Marstorp et al. [31]. However, further analyses and grid sensitivity studies are necessary to understand the effect of the SGS model on separation prediction for WMLES. The grid resolution study with the isotropic polyhedral grid indicated that improved resolution of the thin layer near the wall yielded good predictions, although this grid resolution extrapolated to more complex configurations appears to be significantly computationally expensive for widespread use in the community. The top boundary and spanwise confinement effects were reported, and both affect the size of the predicted separation bubble by $\approx 5\%$ for this case.

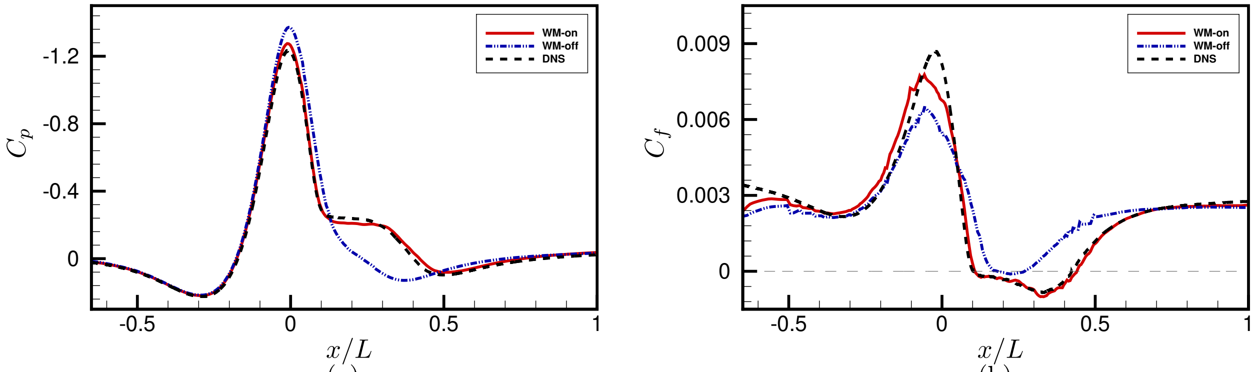

(a) (b)

Figure 12: The variation of (a) wall pressure and (b) skin friction is compared to DNS for polyhedral 25M grid showing the effect of turning off the equilibrium wall model.

Finally, turning off the wall model on the same grid caused the separation bubble to disappear, indicating the effectiveness of the wall model in predicting separation.

# Acknowledgements

This research is sponsored by the NASA Transformational Tools and Technologies (TTT) Project of the Transformative Aeronautics Concepts Program under the Aeronautics Research Mission Directorate. The work of the first author was sponsored by NASA under cooperative agreement NNL09AA00A. We thank Cascade Technologies for providing the CharLES solver and consultation in use of the code, and Dr. Ali Uzun for providing the DNS data and for useful discussions. Computational resources supporting this work were provided by the NASA High-End Computing (HEC) Program through the NASA Advanced Supercomputing (NAS) Division at Ames Research Center. We thank Ponnampalam Balakumar, Kyle Anderson and Steven Bauer for comments on the manuscript.

# References

[1] W Cabot and P Moin. Approximate wall boundary conditions in the large-eddy simulation of high Reynolds number flow. *Flow, Turbulence and Combustion*, 63(1–4):269–291, 2000.

[2] U Piomelli and E Balaras. Wall-layer models for large-eddy simulations. *Annual Review of Fluid Mechanics*, 34(1):349–374, 2002.

[3] J Larsson, S Kawai, J Bodart, and I Bermejo-Moreno. Large eddy simulation with modeled wall-stress: recent progress and future directions. *Mechanical Engineering Reviews*, 3(1):15–00418, 2016.

[4] S T Bose and G I Park. Wall-modeled large-eddy simulation for complex turbulent flows. *Annual Review of Fluid Mechanics*, 50(1), 2018.

[5] P R Spalart. Detached-eddy simulation. *Annual Review of Fluid Mechanics*, 41:181–202, 2009.

[6] S Deck. Zonal-detached-eddy simulation of the flow around a high-lift configuration. *AIAA Journal*, 43(11):2372–2384, 2005.

[7] P R Spalart, S Deck, M L Shur, K D Squires, M K Strelets, and A Travin. A new version of detached-eddy simulation, resistant to ambiguous grid densities. *Theoretical and Computational Fluid Dynamics*, 20(3):181–195, 2006.

[8] M L Shur, P R Spalart, M K Strelets, and A K Travin. A hybrid RANS-LES approach with delayed-DES and wall-modelled LES capabilities. *International Journal of Heat and Fluid Flow*, 29(6):1638–1649, 2008.

[9] J. P. Slotnick. Integrated CFD validation experiments for prediction of turbulent separated flows for subsonic transport aircraft. NATO Science and Technology Organization, Meeting Proceedings RDP, STO-MP-AVT-307, 2019.

[10] O Williams, M Samuell, E S Sarwas, M Robbins, and A Ferrante. Experimental Study of a CFD validation test case for Turbulent Separated Flows. AIAA Paper 2020-0092, 2020.

[11] P D Gray, I Gluzman, F Thomas, T Corke, M Lakebrink, and K Mejia. A new validation experiment for smooth-body separation. AIAA Paper 2021-2810, 2021.

[12] A Uzun and M R Malik. High-fidelity simulation of turbulent flow past Gaussian bump. *AIAA Journal*, 60(4):2130–2149, 2022.

[13] A Uzun and M R Malik. Simulation of a turbulent flow subjected to favorable and adverse pressure gradients. *Theoretical and Computational Fluid Dynamics*, 35(3):293–329, 2021.

[14] R Balin, K E Jansen, and P R Spalart. Wall-modeled LES of flow over a Gaussian bump with strong pressure gradients and separation. AIAA Paper 2020-3012, 2020.

[15] M L Shur, P R Spalart, M K Strelets, and A K Travin. Direct numerical simulation of the two-dimensional speed bump flow at increasing reynolds numbers. *International Journal of Heat and Fluid Flow*, 90:108840, 2021.

[16] P S Iyer and M R Malik. Wall–modeled large eddy simulation of flow over a wall–mounted hump. AIAA Paper 2016–3186, 2016.

[17] P S Iyer, G I Park, and M R Malik. Wall–modeled large eddy simulation of transonic flow over an axisymmetric bump with shock-induced separation. AIAA Paper 2017-3953, 2017.

[18] P S Iyer and M R Malik. Large-eddy simulation of axisymmetric compression corner flow. AIAA Paper 2018-4031, 2018.

[19] P S Iyer and M R Malik. Wall-modeled LES of flow over a Gaussian bump. AIAA Paper 2021-1438, 2021.

[20] M P Whitmore, K P Griffin, S T Bose, and P Moin. Large-eddy simulation of a Gaussian bump with slip-wall boundary conditions. Annual Research Briefs, Center for Turbulence Research, Stanford University, 2021.

[21] R Agrawal, M P Whitmore, K P Griffin, S T Bose, and P Moin. Non-boussinesq subgrid-scale model with dynamic tensorial coefficients. arXiv preprint arXiv:2202.05502, 2022.

[22] Y Khalighi, F Ham, J Nichols, S Lele, and P Moin. Unstructured large eddy simulation for prediction of noise issued from turbulent jets in various configurations. AIAA Paper 2011-2886, 2011.

[23] G I Park and P Moin. Numerical aspects and implementation of a two-layer zonal wall model for les of compressible turbulent flows on unstructured meshes. *Journal of Computational Physics*, 305:589–603, 2016.

[24] G A Bres, S T Bose, M Emory, F E Ham, O T Schmidt, G Rigas, and T Colonius. Large-eddy simulations of co-annular turbulent jet using a Voronoi-based mesh generation framework. AIAA Paper 2018-3302, 2018.

[25] A Lozano-Durán, S T Bose, and P Moin. Performance of wall-modeled LES with boundary-layer-conforming grids for external aerodynamics. *AIAA Journal*, 60(2):747–766, 2022.

[26] A W Vreman. An eddy-viscosity subgrid-scale model for turbulent shear flow: Algebraic theory and applications. *Physics of Fluids*, 16(10):3670–3681, 2004.

[27] M Germano, U Piomelli, P Moin, and W H Cabot. A dynamic subgrid-scale eddy viscosity model. *Physics of Fluids A: Fluid Dynamics*, 3(7):1760–1765, 1991.

[28] P Moin, K Squires, W Cabot, and S Lee. A dynamic subgrid-scale model for compressible turbulence and scalar transport. *Physics of Fluids A: Fluid Dynamics*, 3(11):2746–2757, 1991.

[29] S Kawai and J Larsson. Wall-modeling in large eddy simulation: length scales, grid resolution, and accuracy. *Physics of Fluids (1994-present)*, 24(1):015105, 2012.

[30] J B Freund. Proposed inflow/outflow boundary condition for direct computation of aerodynamic sound. *AIAA journal*, 35(4):740–742, 1997.

[31] L Marstorp, G Brethouwer, O Grundestam, and A V Johansson. Explicit algebraic subgrid stress models with application to rotating channel flow. *Journal of Fluid Mechanics*, 639:403–432, 2009.

[32] A Yoshizawa. Statistical theory for compressible turbulent shear flows, with the application to subgrid modeling. *The Physics of fluids*, 29(7):2152–2164, 1986.

[33] A Rasam, S Wallin, G Brethouwer, and A V Johansson. Large eddy simulation of channel flow with and without periodic constrictions using the explicit algebraic subgrid-scale model. *Journal of turbulence*, 15(11):752–775, 2014.

[34] A Rasam, S Wallin, G Brethouwer, and A V Johansson. Improving separated-flow predictions using an

anisotropy-capturing subgrid-scale model. *International Journal of Heat and Fluid Flow*, 65:246–251, 2017.

[35] G I Park and P Moin. An improved dynamic non-equilibrium wall-model for large eddy simulation. *Physics of Fluids*, 26(1):015108, 2014.